UNIVERSITY OF BIRMINGHAM

SCHOOL OF PHYSICS AND ASTRONOMY

PHYSICS AND TECHNOLOGY OF NUCLEAR REACTORS

MASTER'S THESIS

GRADED SHIELDING AND ITS USE FOR WOUND MONITORS

Author:

Merve Busra Dastan

Supervisor:

Dr. David Forest

In partial fulfillment of the requirements for the degree of

Master of Science in Physics and Technology of Nuclear Reactors

September 2019

Abstract

The aims of this study were to investigate the effect of graded shielding on reducing the background radiation which is crucial for a low-level radiation measurement such as wound monitoring and observe a low activity ^{239}Pu gamma-ray spectrum with a graded shielding. The investigation was performed for two different graded shieldings as lead + iron and lead + copper. As a result, it is evaluated that copper is more effective than iron on eliminating characteristic X-rays of lead and it was seen that without graded shielding with copper, it was impossible to observe L shell Uranium X-rays appear on the gamma spectrum of ^{239}Pu. The minimum detectable activity of ^{239}Pu with NaI(Tl) was calculated as 672 ± 20.51 Bq. Finally, the effective dose delivered from the ^{239}Pu source to a wound was determined as 1.99 Sv.

Acknowledgments

My gratitude goes to my supervisor Dr. David Forest who assisted in the formation of ideas and provided invaluable support throughout the study. I am grateful to Dr. Paul Norman who gave me the opportunity to do this Master's degree. I am also grateful to Republic of Turkey Ministry of National Education providing scholarship to me for studying at the University of Birmingham for my MSc. Studies.

Contents

LIST OF FIGURES

LIST OF TABLES

1. INTRODUCTION

In case of a release of radioactive materials into the environment due to nuclear accidents and weapon tests or natural radiation such as cosmic rays and terrestrial radiation, people can be exposed to a number of radionuclides that may get into the body via various channels and distribute to various organs. In the internal dosimetry regulations, the most likely entry of the radioactive materials into the body are considered as inhalation and ingestion while accidentally intakes through wounds and cuts in the skin are generally ignored (Till and Grogan, 2008, p. 393). However, (Suzuki-Yasumoto and Inaba, 1976) argued that skin is the most frequent path for taking radioactive contaminants into the body. Especially, in case of an accident in reprocessing plants when handling of Plutonium, which is synthetic and mainly an alpha emitter, it can get into the body of the workers via the wounds or cuts on the skin. In that case, as (Harduin and Odilon, 1988) described in detail, a wound monitor is used to examine the depth of the radionuclides and amount of the radiation released in the wound.

Since the alpha radiation of Plutonium does not get out of the body and it has very low gamma emission, looking for the Americium-241 gamma-ray which appears on the gamma spectrum of Plutonium has an advantage rather than direct measurement of the Plutonium isotopes (Harduin and Odilon, 1988; Genicot, Hardeman and Oberstedt, 1995). The advantage is, even have already been effectively absorbed in a tissue, the full energy peak of Americium is still visible because of its high intensity. However, any contribution from the background or surrounding to this peak is undesirable because it affects the accuracy of the detected net activity. Therefore, shielding is necessary to reduce background radiation as much as possible. (Revink and Khairi, 2018) implied that lead is generally preferred as a shielding material for background shielding in gamma spectroscopy because of its high density and atomic number. However, it has its own X-ray emission with an energy of around 70 keV which is around the same energy region as the Americium and should be eliminated. Hence, the graded shielding, which has an additional lower Z material inside the lead, is a solution to eliminate the characteristic X-rays from the lead.

Several detection systems can be used when measuring activity in wounds. As (Dimmerling, 2007; Singh et al., 2011) argued that while HPGe detector is used to gauge the depth of contamination because of its high resolution, the NaI(Tl) detector is used to evaluate the amount of contamination thanks to its high efficiency. Also, it is easy to shield and portable.

From this point of view, the aim of this study is twofold: First, it investigates the effect of two different graded shieldings on the background and characteristic X-ray of lead. Second, it observes the energy spectrum of a weak ^{239}Pu source in a graded shielding. While the main shielding is lead, iron and copper were separately lined into it to compare the effects of them on characteristic X-rays of lead.

The rest of the study is organized as follows: Second section explains the theory behind the gamma-ray interactions, origin of characteristic X-rays, inorganic scintillator working principles, limits of detectability and minimum detectable activity (MDA), the importance of background shielding, the idea of graded shielding, and the dose calculations; Third section reveals the methodology of characterization of a NaI(Tl) detector and building of the graded

shieldings and experimental work; Fourth section gives the results and comparisons of two different graded shieldings, and finally the fifth one is the conclusion of the study.

2. THEORY

2.1. Gamma Radiation, Gamma-Ray Interactions, Gamma-Ray Spectroscopy

Gamma-rays are the highest energy part of the electromagnetic radiation and generally originated from the nucleus during a decay process. Their short wavelength results in a probable long-range without an interaction. (National Aeronautics and Space Administration, Science Mission Directorate, 2010).

When a nucleus is in an excited state, it emits gamma radiation to regain its stability via two main ways which are; de-excitation of a nucleus, or from annihilation. Additionally, the nucleus ends up in an excited state after beta decay or nuclear reactions and gamma-rays arise following these reactions.

Gamma-rays are uncharged and do not cause direct ionization or excitation in the material, so their interaction with an atomic electron and giving all or some part of the energy to the electron is the only way for them to be able to detect. Gamma-rays interact with matter via three major mechanisms which are defined as; photoelectric absorption, Compton scattering, and pair production. All these processes lead to the complete or partial transfer of gamma energy to the electron energy.

2.1.1. Photoelectric Absorption

In the photoelectric absorption case, a gamma ray photon loses all of its energy and totally disappears after having an interaction with an absorber atom. Because of that reason this mechanism is the most important interaction for gamma ray detection while it gives a full energy peak. The interaction takes place with only atomic electron and this electron mostly comes from the K shell of the absorber atom. This atomic electron is called photoelectron and ejected from the atom with an energy of the difference between the initial photon energy and the binding energy of the atomic electron (Knoll, 2010). Besides, the electron binding energy and the atomic number of the atom, gamma-ray energy plays an important role in the photoelectric absorption probability which is approximately given by (Nelson and Reilly, 1991) as;

$$\tau \propto Z^4/E^3 \tag{2.1}$$

Where τ is the photoelectric mass attenuation coefficient, Z is the atomic number and E is the gamma-ray energy.

From equation (2.1), it is seen that the photoelectric absorption process predominant at low gamma energies (up to several hundred keV) and the probability of interaction increases with an increasing atomic number of absorbers. For that reason, high Z materials are chosen for gamma ray shielding and as materials of gamma-ray spectroscopy detectors.

Figure 1 shows the relative importance of the three main types of gamma ray interactions.

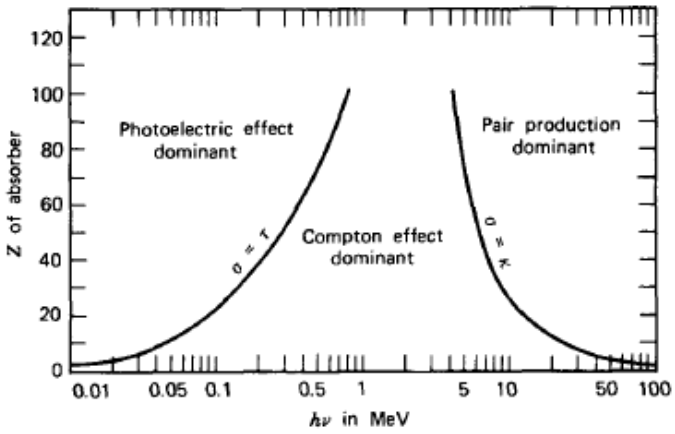

Figure 1. The Relative Importance of the Three Major Types of Gamma-Ray Interactions

2.1.2. Compton Scattering

Compton Scattering always takes place for general gamma ray energies of radioisotope sources. Although this mechanism occurs at any energy region, the reason for indicating a Compton effect dominant region in Figure 1 (Evans, 1955) is the other processes become dominant at low energy (photoelectric absorption) and high energy (pair production) regions. This mechanism takes place between a gamma-ray photon and a valence shell electron of an atom. As shown in figure 2 (Evans, 1955), photon hits the electron then gives an amount of its energy to the recoil electron and both of them scatter with different angles related to the initial direction of the photon. While the wavelength and energy of scattered photon may vary, the momentum and total energy are conserved.

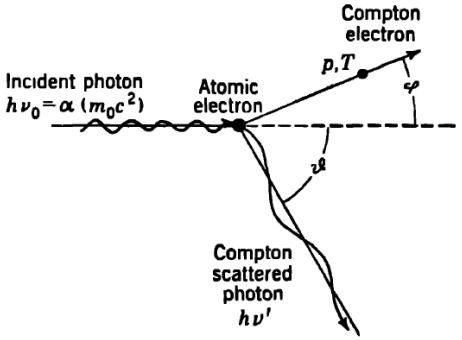

Figure 2. Compton Scattering Between a Photon and an Atomic Electron

The energy of scattered photon $h\upsilon'$ in terms of its scattering angle ϑ is given by the equation (2.2),

$$h\upsilon' = \frac{h\upsilon}{1 + \frac{h\upsilon}{m_0 c^2}(1 - cos\vartheta)} \tag{2.2}$$

where m_0c^2 is the rest mass-energy of the electron which is 0.511 MeV. The kinetic energy of the recoil electron is,

$$E_{e^-} = h\upsilon - h\upsilon' = h\upsilon\left(\frac{(h\upsilon/m_0c^2)(1-cos\vartheta)}{1+(h\upsilon/m_0c^2)(1-cos\vartheta)}\right) \tag{2.3}$$

In general, all scattering angles happen inside the detector. The shape of the distributions of Compton recoil electrons for several different values of incident gamma ray energy is illustrated in Figure 3 (Knoll, 2000). It is also shown that the two cases: on one hand when ϑ is equal to zero, the Compton electron has very little energy. On the other hand, when a head-on collision happens, ϑ becomes equal to π and in this case, recoil electron gets the maximum energy. This cut-off is named as Compton edge.

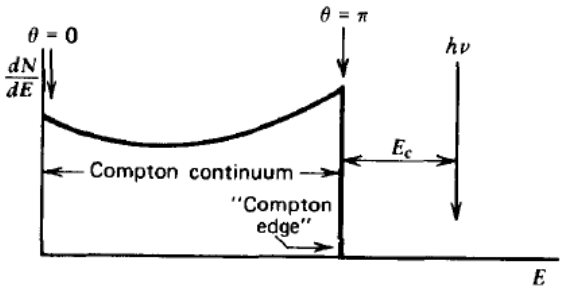

Figure 3. Compton Continuum in Gamma Spectroscopy

2.1.3. Pair Production

Inside the Coulomb field close to the nuclei, the pair production process happens when the incoming gamma-ray photon energy exceeds twice the rest-mass energy of an electron (1.02 MeV). In this process, the photon disappears and an electron-positron pair takes place. Then they share the excess energy which is the difference between the initial gamma photon energy and doubles of the rest mass-energy. The secondary products of this mechanism are annihilation photons whose energy is equal to the rest mass energy and produced by a low energy positron combined with an ordinary electron in the medium. When both annihilation photons absorbed in the detector, full energy peak appears in the detector, if one of them escapes while the other one totally absorbed in the detector, 511 keV will be lost from the detector and remained photopeak is called single escape peak, if both of them escape, the double escape peak shows up in the spectrum (Knoll, 2010).

2.1.4. Gamma-Ray Spectroscopy

In many applications of radiation detectors, the aim is to measure the energy distribution of the incident radiation. These attempts are named as radiation spectroscopy and for different types of radiation spectroscopies, specific detectors are chosen. In order to acts as a gamma spectrometer, a detector should have two capabilities; First, it must be a conversion medium to allows gamma ray photon to interacts and provides one or more fast electrons and second, it must be an ordinary detector for these secondary electrons whose minimum dimension is about a centimeter.

Gamma-ray spectroscopy is combined with different elements such as power supply, detector, preamplifier, amplifier, oscilloscope, multichannel analyzer (MCA) and computer.

When a charge is created in the detector medium, preamplifier takes the low-level output signal from the detector and integrates the charge to sends it to the amplifier. The amplifier increases the pulse and makes it a Gaussian pulse (unipolar) or differentiated Gaussian (bipolar). After amplifier, the pulse now is suitable for the input of an analog to digital converter (ADC) which converts the unipolar or bipolar pulse into digital signals to be able to read by a computer. (https://www.techopedia.com/definition/572/analog-to-digital-converter-adc, 2019).

Multichannel analyzer represents the energy spectrum of the radiation whose an internal ADC evaluates the pulses according to their pulse height that is proportional to the energy of the radiation and stores a spectrum of these pulse heights. With an oscilloscope, one can see the resulting waveform of the charge.

An example diagram of a typical gamma spectrometer is given in figure 4.

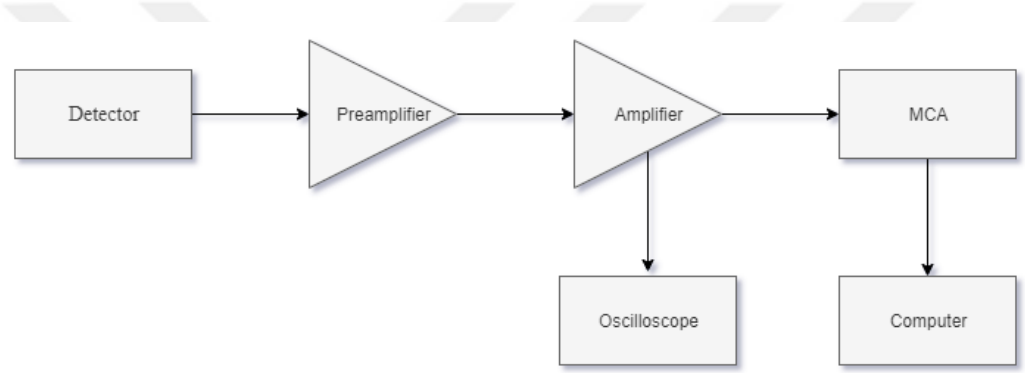

Figure 4. An Example Diagram of a Typical Gamma Spectrometer

In addition, for the same incoming radiation, the energy spectrum may vary with the detector size. On one hand, if the size is small in an extreme case, after some Compton events, both annihilation photons escape and double escape peak appears on the Compton continuum, on the other hand, if it is too large, all interactions happen and all energy is deposited inside the detector and it gives just the photo-peak or full energy peak. This case is impossible in practice because an infinite size detector is needed to get only the full energy peak.

Moreover, all practical detectors are intermediate in sizes and in addition to small detectors, some photons may escape after multiple Compton events and for high energies, both annihilations photons may escape or just one of them may escape from the detector which results in double and single escape peaks on the Compton Continuum.

The illustration of interaction inside the intermediate size detector and energy spectra for low and high energies are given in Figure 5 (Knoll, 2010).

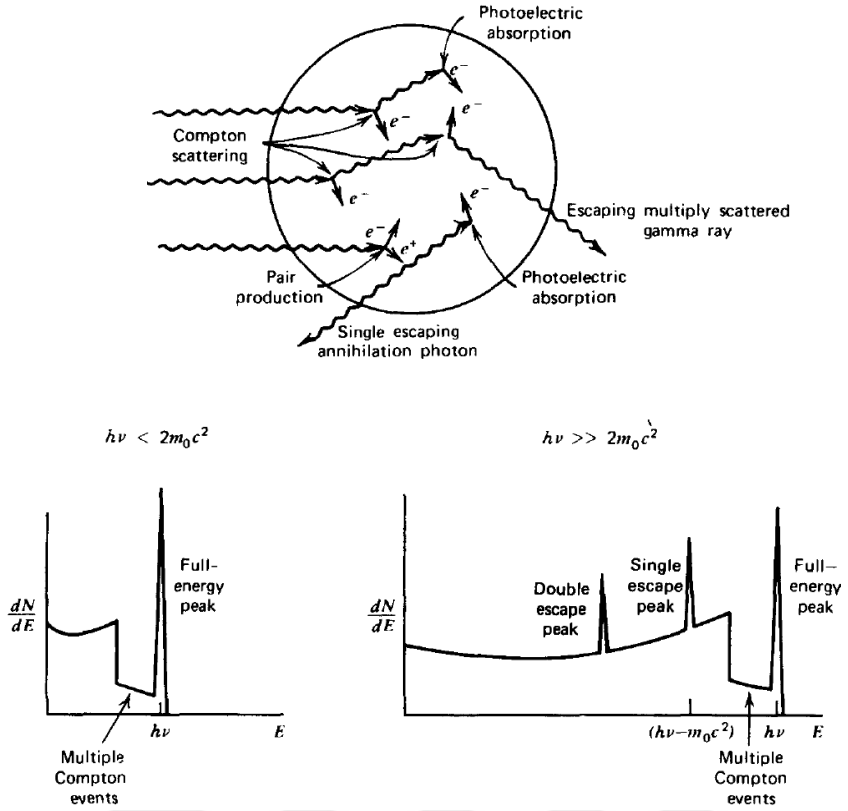

Figure 5. Gamma-Ray Interactions and Energy Spectra for an Intermediate Size Detector

The summary of interactions and energy spectra for different detector size and varying incident gamma ray energy is given in Table 1.

Table 1. The Summary of Energy Spectrum with Varying Detector Size and Gamma Ray Energy

	Gamma-Ray Spectra for Different Detector Sizes		
Incident Gamma-Ray Energy	**Small Detector**	**Big Detector**	**Intermediate Detector**
Low (< $2mc^2$)	Photoelectric absorption and single Compton scattering results in Compton Continuum and full energy peak	Only a full energy peak	In addition to the single Compton scattering and full energy peak, multiple Compton events contribute to the spectrum
Sufficiently High (Several MeV)	Addition to low energy spectrum, after pair production, only a double escape peak forms on the Compton continuum	Only a full energy peak	Addition to the low energy spectrum, after pair production, both single and double escape peaks appear on the Compton Continuum

2.1.5. Energy Calibration, Resolution and Detector Efficiency

Calibration

Energy calibration provides information about the relationship between the known radioisotopes radiation energies and the channel number of the incoming radiation. This information is then used for identifying the unknown source or energy. In addition, the calibration plot should be linear as much as possible to give more accurate results and the accuracy increases with the number of samples and variation of energy intervals.

Energy Resolution

The energy resolution is an important definition in radiation spectroscopy which can be examined by noting a detector response to monoenergetic radiation. The definition of resolution is basically related to the ability to identify two close peaks separately which can be done by decreasing the width of the peak.

The response function which is a differential pulse height distribution provides the information of how much good is the resolution of a detector. Narrower peaks mean that resolution is better and as long as the fluctuations increase and make the peak wider, the resolution decreases. Another general term is full width at half maximum (FWHM) is shown in Figure 6 (Knoll, 2010) and is defined as the width of the distribution at a level that is just half the maximum ordinate of the peak and is used for determining the energy resolution which is a dimensionless number and calculated as the FWHM divided by the centroid of the peak.

Scintillation detectors generally show an energy resolution in the range of 5-10% when used in gamma ray spectroscopy (Knoll, 2010).

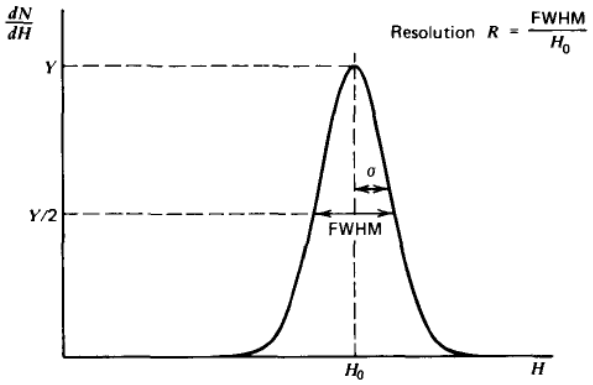

Figure 6. Illustration of FWHM and Resolution

In many cases, the statistical broadening is the most effective reason for resolution loss. In that case, it is predicted that the FWHM is proportional to the square root of the gamma energy. Therefore, the resolution is inversely proportional to the square root of gamma ray energy (Knoll, 2010)

$$R = \frac{FWHM}{H_0} = K\frac{\sqrt{E}}{E} = \frac{K}{\sqrt{E}} \tag{2.4}$$

$$lnR = ln\,K - \frac{1}{2} lnE \tag{2.5}$$

Where K is a constant, R is the resolution and E is the energy. Equation (2.5) provides that the slope of ln R versus Ln E plot should be equal to -0.5.

Detection Efficiency

Charged particles interact with the medium easily and give all their energy and it gives 100% detection efficiency. However, uncharged particles can travel long distances without an interaction which is necessary for detection. This gives a detection efficiency less than 100% which related to the number of pulses recorded to the number of radiation incident on the detector.

(Knoll, 2010) subdivides the detection efficiency into two categories as given below;

$$\epsilon_{abs} = \frac{number\ of\ pulses\ recorded}{number\ of\ radiation\ quanta\ emitted\ by\ source} \tag{2.6}$$

$$\epsilon_{int} = \frac{number\ of\ pulses\ recorded}{number\ of\ radiation\ quanta\ incident\ on\ detector} \tag{2.7}$$

$$\epsilon_{\text{abs}} = \frac{\epsilon_{\text{int}} \times \Omega}{4\pi} \tag{2.8}$$

$$\epsilon_{\text{int}} = \text{N}\frac{4\pi}{\text{S} \times \Omega} \tag{2.9}$$

Where ϵ_{int} is the intrinsic peak efficiency, N is the net area under the peak, Ω is the solid angle (in steradians) subtended by the detector at the source position.

$$\Omega = 2\,\pi\left(1 - \frac{\text{d}}{\sqrt{\text{d}^2 + \text{a}^2}}\right) \tag{2.10}$$

where the source-detector distance (d) and detector radius (a) are shown in Figure 7;

Figure 7. Illustration of Solid Angle

S is the absolute activity of a radioactive source which is;

$$\text{S} = \text{S}_0 \text{e}^{-\frac{\log 2}{\text{t}_{1/2}}\text{t}} \tag{2.11}$$

Where S_0 is the initial activity, $t_{1/2}$ is the half-life of the source, t is the time difference between the date of the experiment and the date of initial measurement.

2.2. Characteristic X-Rays

In the electron cloud, there are electron shells mainly categorized as K, L and M shells. The closest one to the atom is the K shell whose ionization energy is the highest in the atom. When an electron ejected from a shell, it leaves a vacancy behind it and this vacancy is filled by an outer shell electron. During this transition, X-rays are emitted from the atom with an energy of the difference between ejected and filling electrons. When a vacancy occurs in the K-shell, after filling of that vacancy from the other shells, characteristic K X-ray emitted from the atom. If that filling electron comes from the L shell, X-ray is named as K_α with an energy of the difference between K and L shells, or with a lower probability, if it comes from the M shell, K_β X-ray is liberated with higher energy. These emitted X-rays are called characteristic X-rays because every element has its own X-ray energy.

Figure 8 (https://myscope.training/legacy/analysis/eds/xraygeneration/characteristic/, 2019) illustrates the electron transitions between K and L shells.

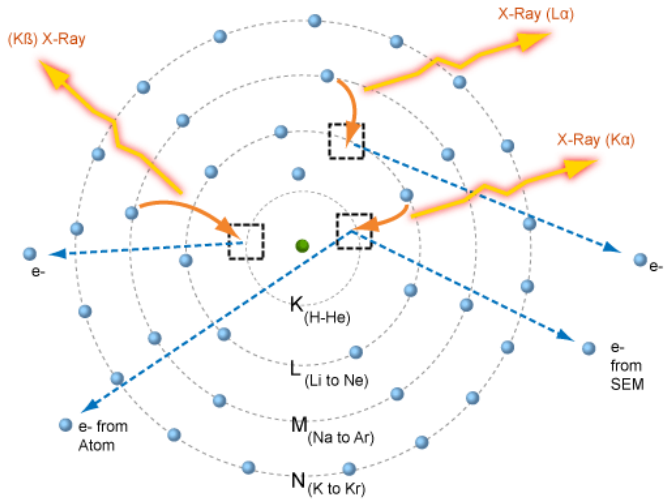

Figure 8. The Illustration of Electron Transitions between K and L Shells

Internal conversion and electron capture can lead to characteristic X-ray emission. In addition, when fast electrons pass through an absorber, atoms generate X-rays after rearranging their electron shells. Also, when exciting radiation interacts with a target material, characteristic X-rays are produced. This is a typical case for shielding materials such as lead or iron. Emitted X-ray energy depends on the atomic number of the target material so the higher atomic number gives the higher energy X-rays. The energy of K Shell X-rays depends on the Z^2 of the target material (Kuhn, 1969).

2.3. Inorganic Scintillators and NaI(Tl) Detector

One of the oldest techniques of detection of ionizing radiation is the use of scintillation light production. In 1947, J.W. Coltman and F.H. Marshall recorded the successful phototube detection of light scintillation produced by radiation of alpha beta and gamma radiation which is the first step of modern scintillation counting. After Hartmut Kallmann's discovery of the

organic scintillators which are generally chosen for beta spectroscopy and detection of fast neutrons, Robert Hofstadter discovered the scintillations of inorganic materials and decided that the NaI (sodium iodide) is the best one to work with (Theodorsson, 1996).

Inorganic scintillators are generally used for gamma-ray spectroscopy since they have a high atomic number and high density. A good scintillation material must have some characteristics as follows;

- High ability to transform charged particles' absorbed kinetic energy into detectable light.
- The medium should be transparent to its own light.
- The short decay time of induced luminescence.
- Light yield should change linearly with deposited energy.
- When used for gamma detection, the probability of photon absorption must be high.

It is hard to find a material that possesses all of the above criteria, therefore, one must have a concession while choosing a scintillation material. Although there are a number of inorganic scintillation detectors such as CsI(Tl) (thallium doped cesium iodide), CsI(Na) (sodium doped cesium iodide) and LiI(Eu) (europium doped lithium iodide) and $CeBr_3$ (cerium bromide), $LaBr_3$(Ce) (cerium doped lanthanum bromide) and $LaCl_3$(Ce) (cerium doped lanthanum chloride) the most widely used one is the NaI(Tl) (thallium doped sodium iodide) because its light output and linearity is the highest.

2.3.1. Working Principles of Scintillator Detectors

Solid material has energy levels of atoms that produce a group of levels called bands. One of them named as valence band which is completely full of electrons, the other one is the conduction band where electrons can move freely through a lot of empty levels. Also, there is an energy level between these two bands in which electrons can never be found in a pure crystal called a forbidden gap. As a result of absorption of energy in the crystal, electrons are promoted from valence band to the conduction band leaving behind a hole in the valence band.

Pure crystal such as NaI and CsI are efficient scintillators but due to the necessity of low temperature and UV transmission, they are not widely used. Also, in pure crystal, electrons may return to the valence band with a photon emission which is ineffective since the emitted photon energy is too high from visible range. Therefore, small amounts of heavy metal impurities such as thallium (Tl) and europium (Eu) are generally added to the inorganic scintillators with the aim of increasing the probability of visible photon emission. These impurities are called activators, make the forbidden gap suitable for electrons to de-excite back to the valence band by creating special sites called as luminescence centers in the forbidden gap. Since the electron energy is less than the total forbidden gap (Knoll, 2010).

Figure 9 illustrates the energy level structure of an activator center in detail. The scintillation process starts with the production of excitons, which are weakly coupled electron-hole pairs and their energy level is just below the conduction band, and ion pairs. In addition, there is an activator ground state in the lower half of the forbidden gap and first excited state in the top half. A positive ion in the valence band easily captures an electron in the activator ground state which results in a formation of positive ion in the activator. Then, this positive ion captures a free electron in the conduction band and also tends to capture excitons and UV photons and this speeds up the recombination process giving good timing resolution. In all cases, the resulting excited activator atom de-excites to the ground state by emitting a photon. This transition energy is much smaller than the whole forbidden gap and the emitted photons from this process don't have enough energy to excite electrons directly from the valence band to conduction band, so the crystal is transparent to these photons which in the visible range that is required for scintillation process (Tait, 1980).

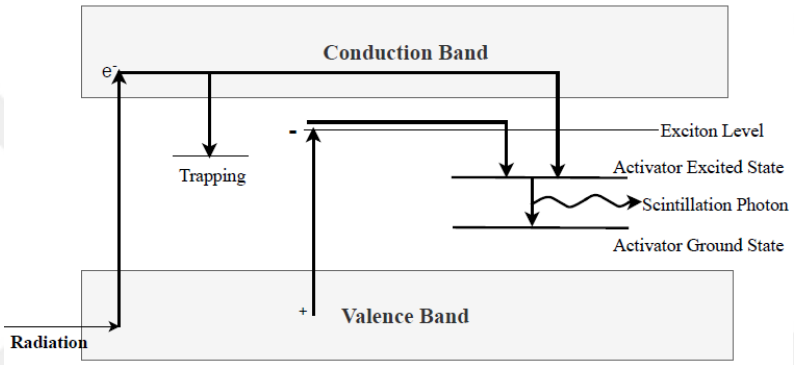

Figure 9. Scintillation Process in Extrinsic Inorganic Crystals

Scintillation counter systems consist of three main units are scintillator, photomultiplier and associated electronic system. The scintillation process starts when secondary electrons or charged particles ionizes and excites the atoms of detector the medium. Although scintillators deposit most of the energy as heat, for a short time, some part of this energy is captured in higher energy levels and fluorescent light is emitted through de-excitation process which is detected by a photomultiplier tube (Theodorsson, 1996).

Figure 10 (Theodorsson, 1996) illustrates the NaI(Tl) scintillation detector unit. The NaI crystal absorbs the energy of charged particles through ionization and excitation and part of this energy is transformed into light.

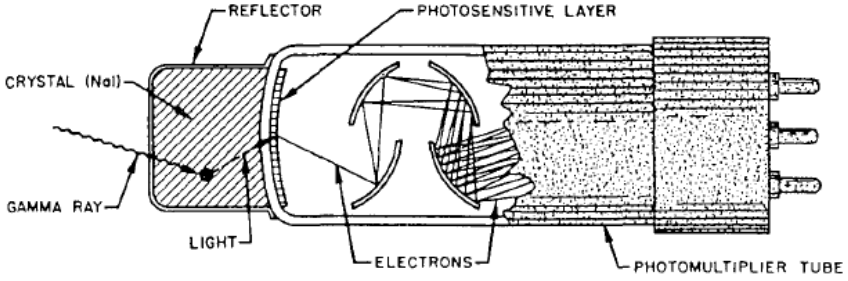

Figure 10. The Scintillation Unit of NaI Detector

2.4. Limits of Detectability and Minimum Detectable Amount (MDA)

While working with low-level radioactivity, it is important to distinguish the original weak signal from the possible signal that comes from the statistical errors of the electronic system or background. The reliable smallest signal intensity should be known to set a detection limit. In addition, while monitoring the possible radioactive contaminants, the certain minimum detectable amount (MDA) of radioactivity should be measurable since it is required by some regulatory agencies.

(Currie, 1968) defined the most widely used definition of MDA that is based on arbitrary choices of $P_D = 0.95$ and $P_{FA} = 0.05$ where P_D is the detection probability and P_{FA} is the false alarm probability. In the simplest case;

$$N_S = N_T - N_B \tag{2.12}$$

Where, N_T is the number of total counts, N_B represent the number of counts for background and N_S is the true net number of counts.

To understand whether the sample contains activity N_S is compared with the critical level L_C which is a determined value and named as the threshold or alarm level. Basically, if N_S is less than L_C, it means the sample does not contain radioactivity, or if N_S exceeds L_C, some real activity must be present. If it is assumed that the counting time is long enough and the number of counts for each measurement is high, then both N_T and N_B should follow Gaussian distributions. From equation (2.12) N_S should also follow a Gaussian distribution and its standard deviation σ^2 is;

$$\sigma_{N_S}^2 = \sigma_{N_T}^2 + \sigma_{N_B}^2 \tag{2.13}$$

2.4.1. No Source Is Present

If there is no real activity present in the sample, the net counts only come from the background which means N_T is equal to the N_B and $\sigma_{N_T} = \sigma_{N_B}$. Also, the mean value of N_S is zero. The standard deviation of the net counts is given below,

$$\sigma_{N_S} = \sqrt{2\sigma_{N_B}^2} = \sqrt{2}\sigma_{N_B} \tag{2.14}$$

If the counting statistics is the only fluctuations entering the measurement, then $\sigma_{N_B} = \sqrt{N_B}$ and $\sigma_{N_S} = \sqrt{2N_B}$.

With the absence of a source, any positive indication is a false positive as shown in Figure 11. So L_C should be set as high as possible to ensure that the case of N_S *exceeds* L_C is acceptably small. As given in table 7 (Knoll, 2010) (see Appendix), the probability of a random sample from the Gaussian distribution having the value within the interval of the mean $\pm 1.64\sigma$ is 90%. Because the only concern is the positive deviations from the mean, a random sample lies below the mean $+1.64\,\sigma$ with a probability of 95%.

$$L_C = \overline{N_S} + 1.64\sigma_{N_S} = 1.64\,\sqrt{2}\sigma N_B = 2.33\sigma_{N_B} \tag{2.15}$$

Eq. (2.15) ensures that the probability of getting a false positive is no greater than 5% which is a general setting of L_C. With the distributions expected for the net counts N_S, the false positive case and the false negatives are shown in figure 11 (Knoll, 2010).

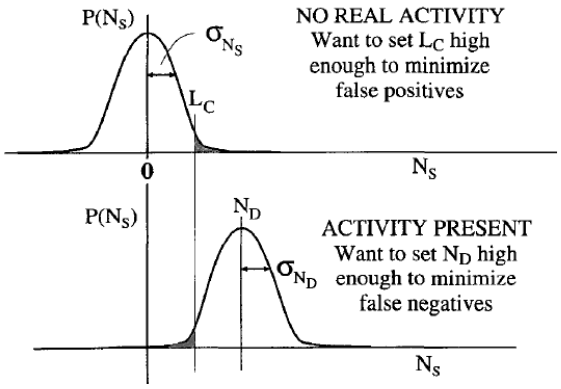

Figure 11. The Cases of Both the Absence and Existence of the Real Activity

2.4.2. Radioactive Source Is Present

In case of a radioactive source is present, the mean value of the N_S is assumed to be positive. Any result from the case of no source is present is accepted as false negatives, to avoid accepting background as a source, N_D should be set high enough but if the level is too high, a possible real activity may be missed which is undesirable. To prevent this, the false negative probability is assumed as 5%.

Let N_D is the minimum net value of N_S,

$$N_D = N_T - N_B \tag{2.16}$$

$$\sigma_{N_D}^2 = \sigma_{N_T}^2 + \sigma_{N_B}^2 = \sqrt{N_T^2} + \sqrt{N_B^2} = N_D + 2N_B \tag{2.17}$$

$$N_D = L_C + 1.64\sigma_{N_D} \tag{2.18}$$

$$N_D = 1.64\sqrt{2}\sigma N_B + 1.64\sqrt{N_D + 2N_B} \tag{2.19}$$

As a result N_D becomes,

$$N_D = 4.65\sqrt{N_B} + 2.71 \tag{2.20}$$

Eq. (2.20) is called the Currie equation where N_D is the minimum mean number of counts needed from the source to ensure a false negative rate no larger than 5% when the system is operated with a critical level.

To calculate the minimum detectable activity α, N_D should be converted with additional factors as, f is the radiation yield per disintegration, ϵ is the absolute detection efficiency. T is the counting time per sample (Knoll, 2010).

$$\alpha = \frac{N_D}{f\epsilon T} \tag{2.21}$$

2.5. Background and Detector Shielding

The existence of cosmic radiation and natural environmental radioactivity result in inevitable background detection in every measurement with radiation detectors. This background signal depends on the detector size, its shape, and the possible shielding design. Since the minimum detectable activity depends on the background counts, the detection of it is more significant in low-level counting. Moreover, it is crucial to make this background as low as possible when measuring the radiation of weak sources. This reduction is generally done with an external shielding material for the detector.

Sources of Background radiation are as follows:

- The natural radioactivity of the detector's materials.
- The natural radioactivity of ancillary equipment, supports and shielding around the detector.
- Terrestrial radiation comes from the earth's surface.
- Radioactivity in the air and cosmic radiation (Knoll, 2010).
- If there is another radioisotope nearby, it may contribute radiation to the spectrum.

2.5.1. Shielding Effect on the Background and Gamma-Ray Spectrum

The background in any gamma-ray spectrum varies with the circumstances such as detector size or shielding. The terrestrial and cosmic ray radiation are generally dominant in gamma ray detectors without shielding.

When a shielding material is placed around the detector, it decreases the background; however, it may contribute some secondary radiation from itself to the spectrum. This additional radiation arises from the interaction between initial gamma rays from the source and the shielding material. Significant processes are mainly as follows:

- Compton backscattering of the primary gamma-rays which caused by the Compton scattering with the surrounding materials before the detector. This peak is generally expected at 0.2-0.25 MeV region.
- The formation of the secondary annihilation which may cause confusion in annihilation detection measurements.
- The characteristic X-rays through photoelectric absorption or pair production inside the shielding material.

These possible interactions are illustrated in figure 12.

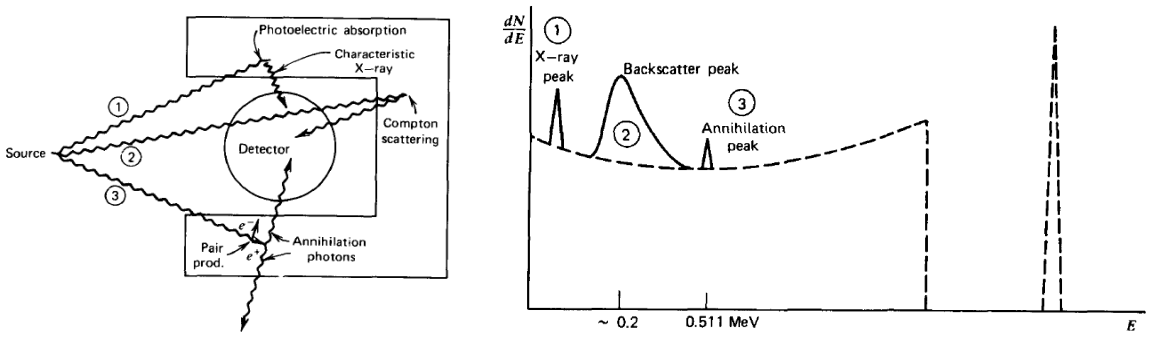

Figure 12. The Additional Possible Interactions Due to a Shielding Material Surrounds the Detector

2.5.2. Low Background Shielding Materials

Lead is generally preferred as a detector shield because of its large atomic number and high density. A few centimeters lead is enough to reduce the natural background effectively. However, due to its high atomic number, the characteristic X-ray from the lead is relatively energetic and penetrable. Also its K_α energy between 70-85 keV.

Iron or steel is another common material in gamma ray shielding. It is generally used with lead when using lead alone is too expensive. On the other hand, due to its lower atomic number and density compared to lead, several tens of centimeters are needed for reduction of low gamma background.

In Table 2 (Firestone, 1996), some characteristics of the shielding materials used in this study are given.

Table 2. Characteristic of the Shielding Materials Used in This Study

Shielding Material	Atomic Number (Z)	Density (g/cm^3)	Dominant Characteristic X-Ray Energy (keV)	Yields	Does it can be detected with NaI(Tl)	Reason
Lead	82	11.34	$K_{\alpha1}$ 74.969 $K_{\alpha2}$ 72.805 $K_{\beta1}$ 84.938 $K_{\beta2}$ 87.300	46.2 27.7 10.7 3.91	Yes	
Iron	26	7.874	$K_{\alpha1}$ 6.403		No	Out of detectable energy range
Copper	29	8.96	$K_{\alpha1}$ 8.047		No	Out of detectable energy range

2.5.3. Graded Shielding

Photoelectric absorption within primary radiation from the source and shielding material results in characteristic X-ray emission from the shielding material. When this X-ray is detected by the detector, it is generally unwanted for low radiation detection measurements.

The graded shielding is composed of different shielding materials that mainly consist of high-Z material. To absorb the X-rays form high Z, different lower Z material is lied into the main shielding. However, this lower Z material also emits lower-energy X-rays of its own. This addition of lower Z materials is repeated until the last emitted X-ray energy is relatively low or out of the interest region and can be ignored.

2.6. General Routes of Intake of ^{239}Pu

Radiation exposure from the ^{239}Pu to the workers can happen both internally and externally in the reprocessing plants or facilities that work with Plutonium isotopes. Whereas external exposure caused by x-rays, gamma rays and neutrons emitted from the ^{239}Pu, internal exposure happens when it is inhaled, ingested or injected. The focus in this study is the injection through a wound or cut on the skin that allows the material go directly into the blood circulation system. Then it can be transferred to the other organs in the body as shown in figure 13 (International Commission on Radiological Protection [ICRP], 1998).

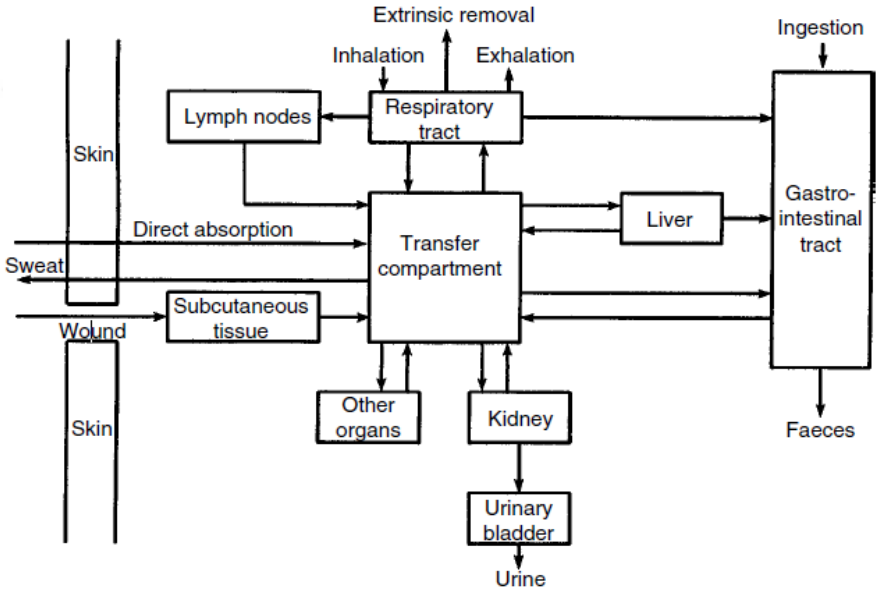

Figure 13. General Routes of Intake and Transfers between Compartments

Figure 13 also demonstrates that when a material is taken into the body from a wound, there many possible organs to pass or retain.

3. METHODOLOGY

3.1. Equipment

- ORTEC (Catalog Number 905-4) NaI(Tl) detector
- CANBERRA Model 2007P Preamplifier
- ORTEC 4001M Minibin Power Suppy
- CANBERRA H.V power supply
- ORTEC Amplifier
- Tektronix TDS2012C Oscilloscope
- MSc Box 1 Gamma Reference Source Set
- ^{239}Pu source (ANS39)
- Maestro Software

3.2. Experimental Setup and Determination of Background

The setup was done as illustrated in Figure 4 and the voltage was increased slowly to prevent any damage to the NaI(Tl) detector and set to 600V. Before taking the spectra for all MSc Box1 sources, which are ^{137}Cs, ^{60}Co, ^{133}Ba, ^{241}Am and ^{152} Eu, the spectrum of background radiation was taken and it is given in Figure 14. For the calibration sources, the pulse was observed on the oscilloscope before Maestro software was started to use.

On the Maestro, to be able to observe a wider spectrum, the coarse gain and fine gain was increased up to the limit of the highest energy gamma ray, which belongs to the ^{152} Eu, can be seen on the spectrum. The reason for choosing a wider spectrum was to increase the ability to observe the lower gamma ray region better. The resulting parameters are given below;

Operating voltage: 600V

Coarse gain: 1K

Fine Gain: 8.9

Shaping Time: 0.5 μs

Real Time: 500 s

Source to detector distance: All sources were mounted against the detector throughout the experiment.

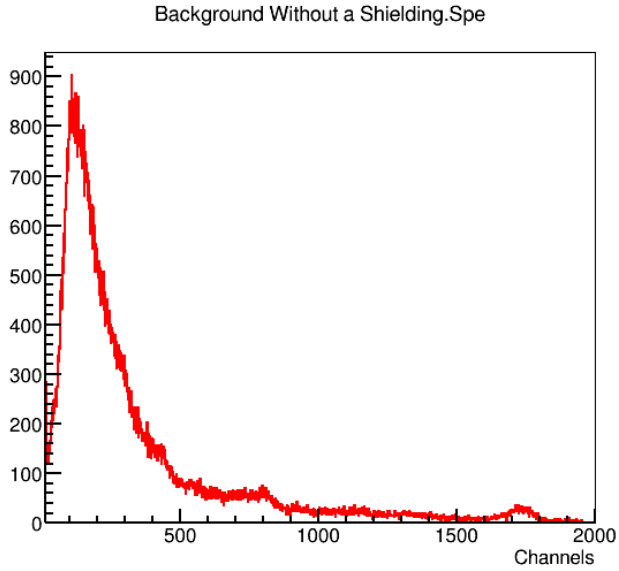

Figure 14. Background Radiation in the Nuclear Laboratory

Figure 14 shows that the background was taken for 500 seconds at 10.07.2019, the terrestrial and cosmic radiation are dominant at low energies. Therefore, this natural radiation should be eliminated to be able to perform low energy and low activity measurement.

3.3. Spectra of the Sources and the Calibration

Gamma-ray energy spectra of ^{137}Cs, ^{60}Co, ^{241}Am, ^{133}Ba and ^{152} Eu are given in figures 15, 16, 17, 18 and 19, respectively.

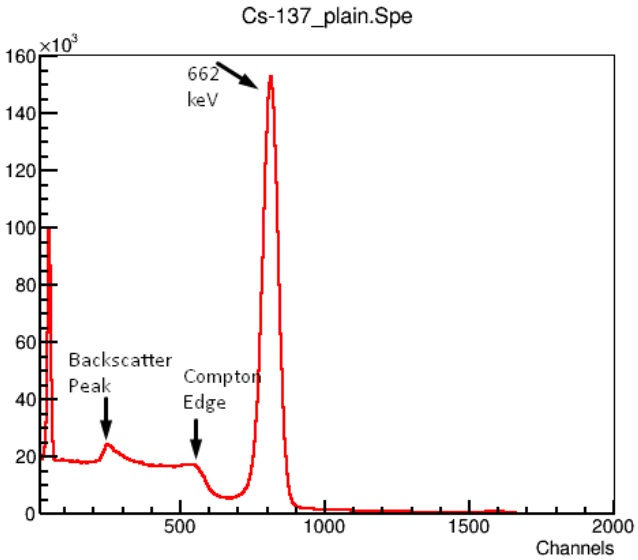

Figure 15. Gamma-Ray Energy Spectrum of ^{137}Cs

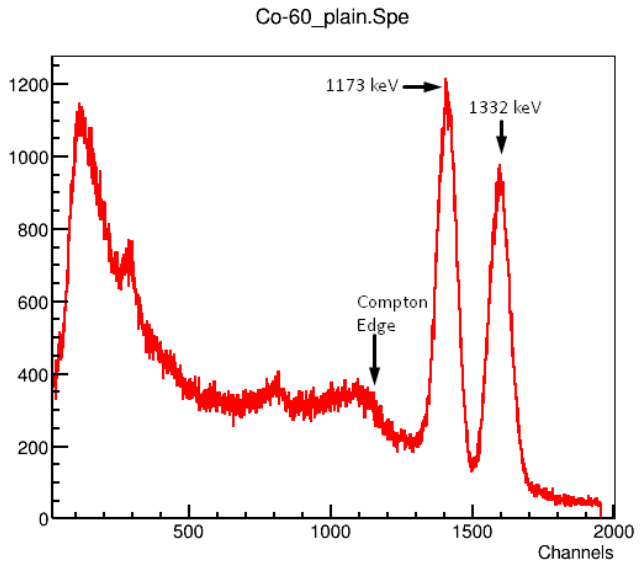

Figure 16. Gamma-Ray Energy Spectrum of ^{60}Co

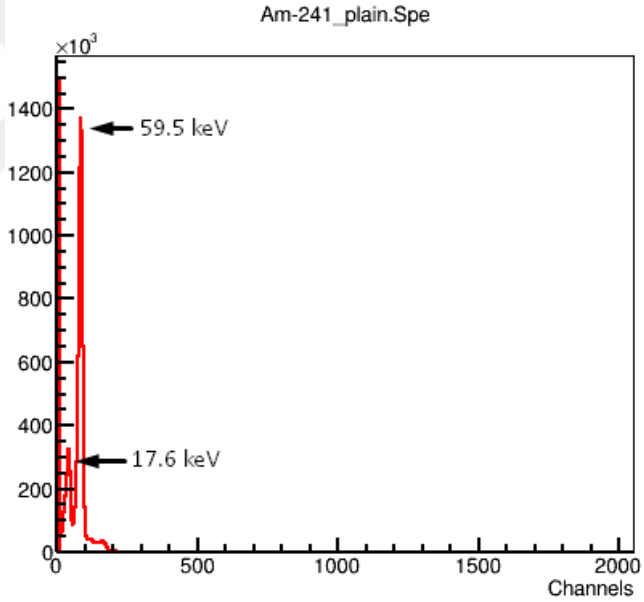

Figure 17. Gamma-Ray Energy Spectrum of ^{241}Am

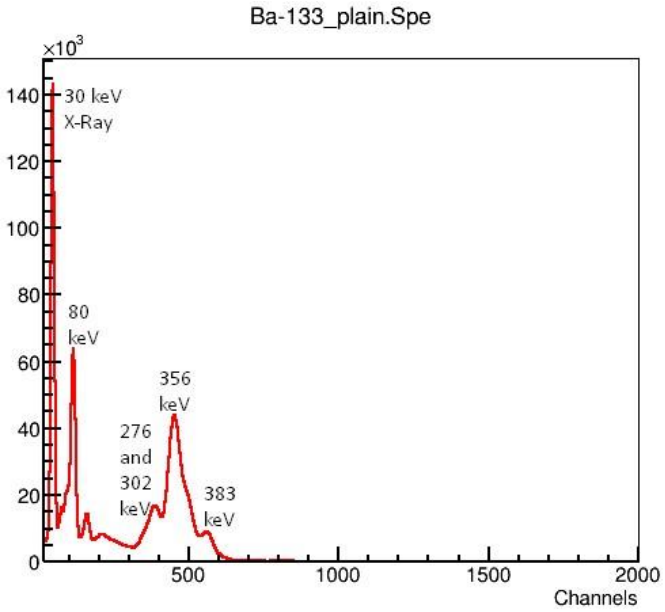

Figure 18. Gamma-Ray Energy Spectrum of ^{133}Ba

As given in figure 18, on the gamma ray spectrum of ^{133}Ba, due to the relatively low resolution, the 276 keV (yield is 7.6) and 302 keV (yield is 18.34) gamma rays are overlapped at the 379. Channel, to find an energy of that channel, the weighted average of these two energies were calculated as;

$$\frac{(276.3989 \times 7.16) + (302.8508 \times 18.34)}{7.16 + 18.34} = 295.42\ keV$$

As a result, the resulting energy for 379. Channel is attributed as 295.42 keV.

The same procedure was applied to a peak of the ^{152}Eu. In figure 19, the 1100 keV on the spectrum is the weighted average of the 1085 and 1112 keV gamma-rays whose yields are 10.11 and 13.67 respectively. The spectrum for ^{152}Eu is given as follows;

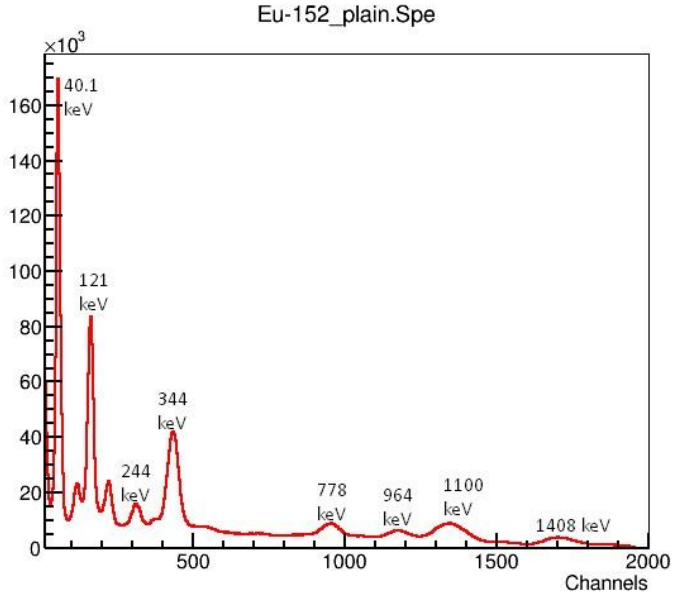

Figure 19. Gamma-Ray Energy Spectrum of ^{152}Eu

After fitting all of the channels for all of the sources by using ROOT Analysis, traditionally, Calibration has been assessed by measuring the channel numbers and the energies of all MSc Box1 sources data and were given in Figure 20. The 'energy = 0.883(centroid) − 14.382' equation will be used to determine the energy of the characteristic X-ray's from the lead shielding and can be used to identify other unknown energies. The error bars were added to the graph but they are so low and invisible because of data points.

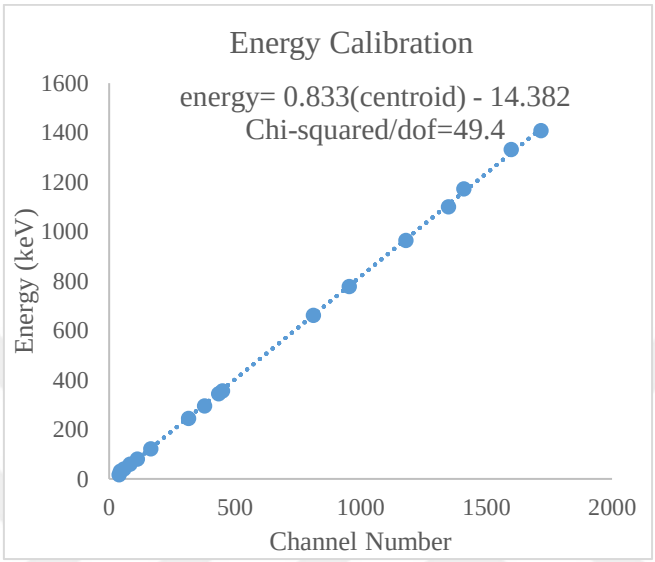

Figure 20. The Energy Calibration

3.4. Characteristics of NaI(Tl) detector

3.4.1. Resolution

The energy resolution of each peak was calculated with equation (2.4) and plotted against the gamma ray energy. In keeping with the theory, the slope of the overall plot was found as -0.5442.

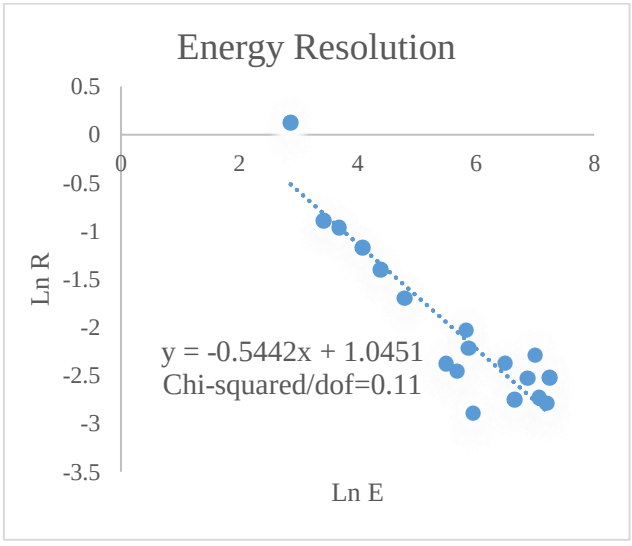

Figure 21. The Energy Resolution in Log Scale

The percentage error on the slope of the resolution is;

$$Percentage\ error = \frac{|0.5442 - 0.5|}{0.5} \times 100 = 8.84\%$$

3.4.2. Detection Efficiency

The absolute and intrinsic efficiencies were calculated according to the procedure used by (Knoll, 2010) which was given in section 2.1.5 for all sources mounted against the detector.

Figure 22 illustrates the NaI(Tl) absolute and intrinsic efficiencies in percent with gamma ray energies. On one hand, at lower energies, probability of gamma ray interaction with the material is the highest., the incoming gamma radiation undergoes an interaction with the first material they meet which is aluminum material covers the mount of the detector instead of the NaI crystal. This issue gives almost zero efficiency at the lowest gamma ray energy. On the other hand, at higher energies, efficiency decreases due to the increase in probability of escaping photons.

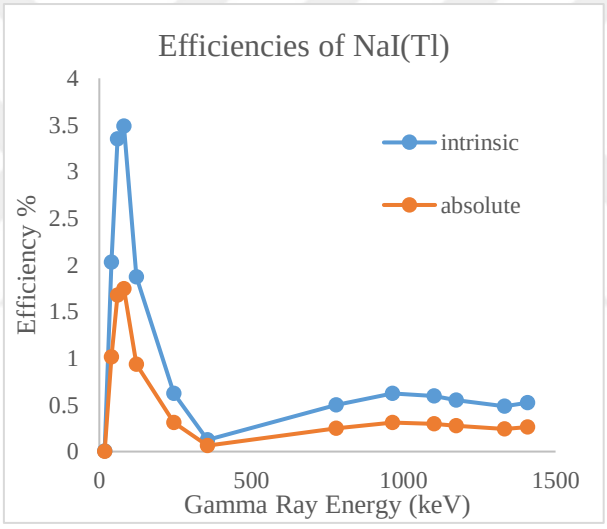

Figure 22. The Intrinsic and Absolute Efficiencies (in Percent) of NaI(Tl) Detector

3.5. Shielding Design with Lead

After taking the background and evaluating the characteristic features of NaI(Tl) detector, shielding design surrounds the detector was started to apply. To reduce the background, the detector sides were covered with lead bricks, which are 20x10x5 cm in dimensions. To cut the contribution of background radiation from the bottom, 6 mm lead plates were added on the table.

Before absolutely shielded the surrounding of the detector, a semi shielding design was created to compare the contribution of characteristic X-rays from the lead gradually.

The first shielding geometry is given in figure 23,

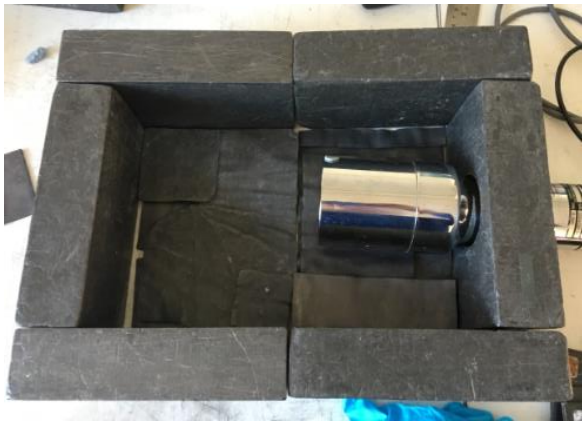

Figure 23. The Semi Shielded Geometry

The energy spectrum of the semi shielded geometry was taken for 900 seconds and is given in figure 24,

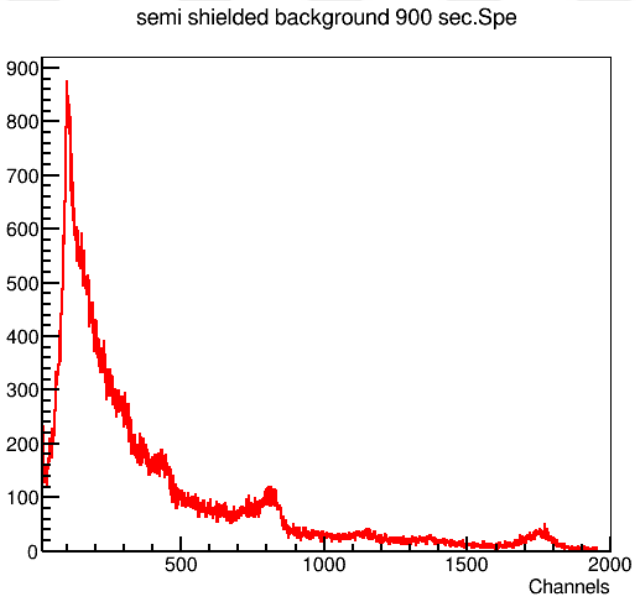

Figure 24. The Background with Semi Shielded Geometry

After taking the background for semi-shielded geometry, the shielding was absolutely closed and improved to 50x25x25 cm in dimension as given in figure 25.

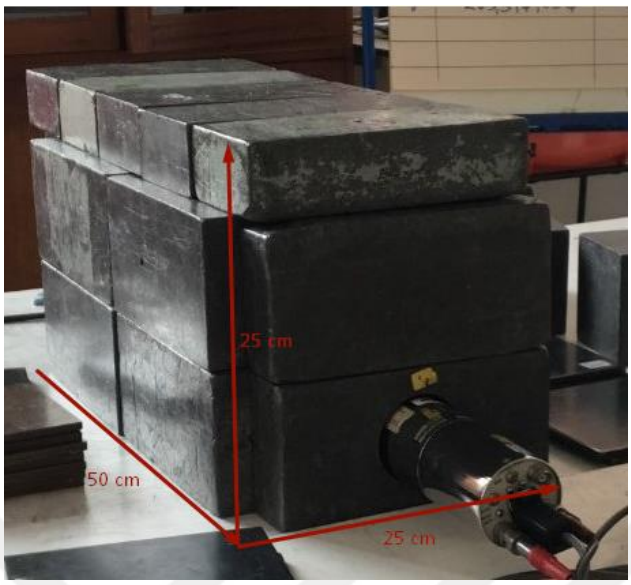

Figure 25. The Geometry of Absolute Shielding

The energy spectrum of the shielded geometry given in Figure 26 was taken for 1 hour.

Figure 26 presents the characteristic X-rays of lead, which needs to be eliminated, very clearly.

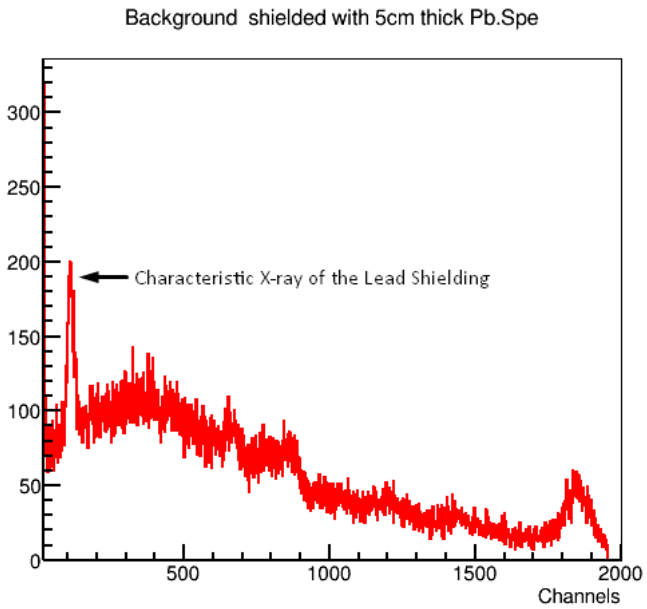

Figure 26. The Energy Spectrum for the Geometry Given in Absolute Shielding

Figure 27 illustrates the fitted characteristic X-ray from the lead is at 112. channel which corresponds to both K_α and K_β X-rays.

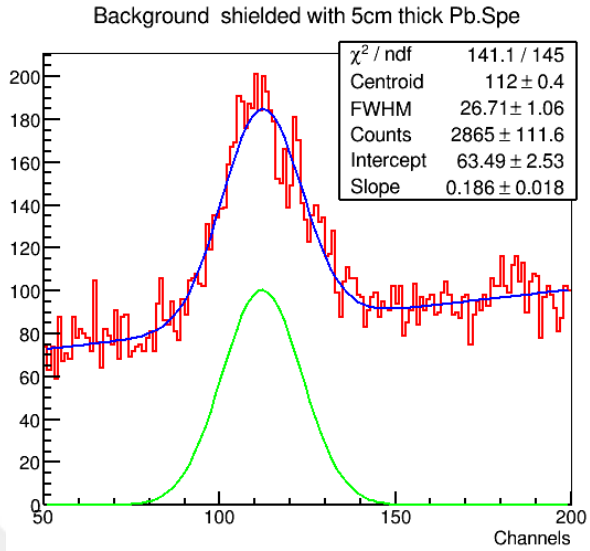

Figure 27. The Fitted X-Ray from the Lead

In order to find the expected energy from the calibration, the weighted averages from both K_α and K_β X-rays, which are given in Table 2, were calculated.

$$K_{\alpha,\beta} = \frac{K_{\alpha,\beta1} \times \gamma_{\alpha,\beta_1} + K_{\alpha,\beta2} \times \gamma_{\alpha,\beta_2}}{\gamma_{\alpha,\beta_1} + \gamma_{\alpha,\beta_2}}$$

The weighted average of K_α;

$$K_\alpha = \frac{74.969 \times 0.462 + 72.805 \times 0.277}{0.462 + 0.277} = 74.158\ keV$$

The yield of that of that K_α,

$$\gamma_{K_\alpha} = \frac{74.969 \times 0.462 + 72.805 \times 0.277}{74.969 + 72.805} = 0.3708$$

The weighted average of K_β;

$$K_\beta = \frac{84.938 \times 0.107 + 87.300 \times 0.0391}{0.107 + 0.0391} = 85.570\ keV$$

The yield of that of that K_β,

$$\gamma_{K_\beta} = \frac{84.938 \times 0.107 + 87.300 \times 0.0391}{84.938 + 87.300} = 0.072$$

When the X-ray was zoomed in the Maestro software the K_α appeared at 107.66. channel and K_β was at 133.51. channel. To find the overall energy of the characteristic X-ray,

$$Pb\ X\ ray\ \frac{74.158 \times 0.3708 + 87.570 \times 0.072}{0.3708 + 0.072} = 76.338\ keV$$

The $y = 0.883x - 14.382$ equation from the calibration, where y is the energy and x is 112, so, the characteristic X-ray from the lead is calculated from the calibration is,

$$y = 78.914 \text{ keV}$$

The percentage error on expected and calculated characteristic X-ray is,

$$Percentage\ error = \frac{78.914 - 76.338}{76.338} \times 100 = 3.374\%$$

3.6. Graded Shielding with Lead and Iron

After observing the effect of lead on background and contribution of its characteristic X-rays, the effect of additional iron shielding on the background and characteristic X-ray from the lead were investigated. The inner shielding, which is 15x15 cm in dimensions and 6 mm in thickness, is given in figure 28. Inner shielding with iron was lined inside the lead shielding except for the bottom and the detector side.

The graded shielding geometry with iron before the top was absolutely shielded is given in figure 28 and the energy spectrum of it was taken for 1 hour.

Figure 28. The Graded Shielding Geometry with Iron

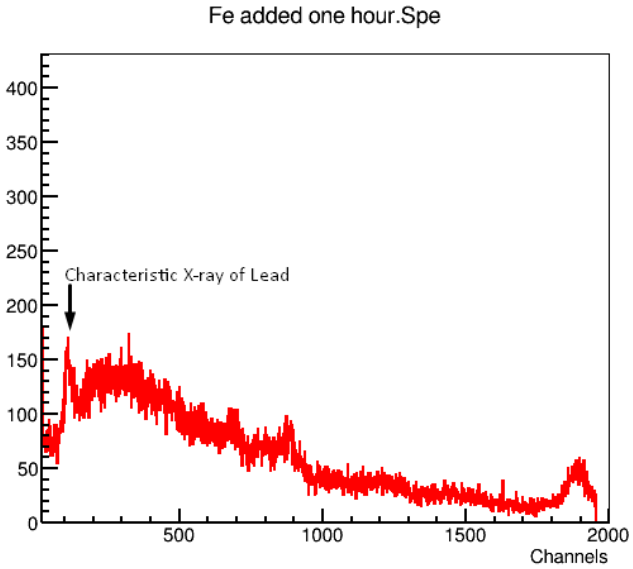

Figure 29. The Energy Spectrum of Background with the Graded Shielding with Iron

It is seen in Figure 29 that iron decreases the contribution of characteristic X-rays of lead.

3.7. Graded Shielding with Lead and Copper

After observing the effect of iron on the characteristic X-rays of lead, shielding geometry changed slightly in order to create a little box from the copper plates. The new lead shielding geometry was 30x25x25 cm in dimensions and the copper plates were 11x11 in dimensions. Because of the new design, the background spectrum inside the lead was taken again before working with the graded shielding with copper.

Figure 30 and 31 indicates the graded shielding geometry with copper before the top was absolutely shielded and the energy spectrum of background taken for 900 seconds inside of it respectively.

Figure 30. The Graded Shielding Geometry with Copper

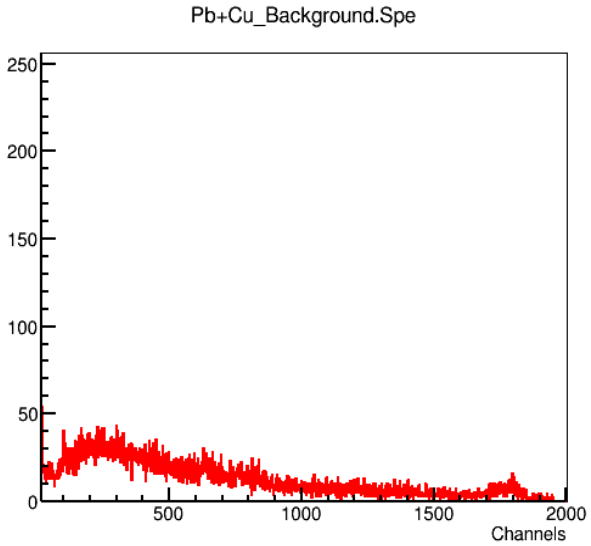

Figure 31. The Background inside the Graded Shielding with Copper

Figure 31 shows the elimination of the X-rays with copper.

3.8. MDA for ^{239}Pu and Gamma Ray Spectrum with Graded Shielding

3.8.1. MDA of the Americium peak

In this part, to check whether the weak Plutonium source gamma spectra can be taken, MDA of the americium gamma peak appears on the gamma spectrum of the ^{239}Pu was calculated with the equations (2.20) and (2.21). For equation (2.20), number of counts for background N_B is 9365980 ±6120. With this information N_D is calculated as;

$$N_D = 4.65\sqrt{N_B} + 2.71 = 4.65\sqrt{9365980} + 2.71$$

$$N_D = 14233 \pm 21.62$$

In equation (2.21), f is 0.3509, ϵ is taken from figure 22 and equal to 1.675 % at 59 keV and T is 3600 sec. When all parameters inserted, MDA is calculated as;

$$\alpha = \frac{\mathrm{N_D}}{f\epsilon T} = \frac{14233}{0.3509 \times 167.5 \times 3600} = 672 \pm 20.51 \text{ Bq}$$

Where the Plutonium source used is 3700 Bq and can be observed easily on the spectrum.

3.8.2. ^{239}Pu Gamma Ray Spectrum with Graded Shielding

After deciding the graded shielding with copper is better than with the iron when eliminating the Characteristic X-rays of the lead, the ^{239}Pu source was put inside the graded shielding with copper and energy spectrum was taken for 1 hour. The spectrum is given in figure 32 and figure 33 is the zoomed version of it.

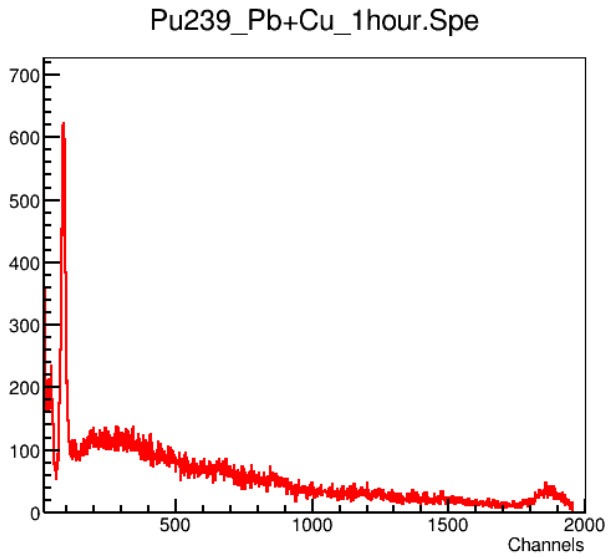

Figure 32. ^{239}Pu Gamma Spectrum inside the Graded Shielding with Copper

^{239}Pu emits alpha particles at 5105.5 keV, 5144.3 keV and 5156.59 keV energies (NNDC, 2019) and transfer into Uranium atom which has an unstable electron configuration and emits X-rays at 13.60 keV, 17.06keV and 20.30 keV with yields of 1.48, 2.09, and 0.49 respectively. These X-rays are accepted as characteristic X-rays from the ^{239}Pu decay process and are named as Uranium L shell X-rays (Browne, 1952). Also, when ^{239}Pu captures two neutrons and forms into ^{241}Pu. Beta decay of ^{241}Pu results in the formation of ^{241}Am.

Figure 33 shows these X-rays and the gamma ray from the ^{241}Am at 59.9 keV.

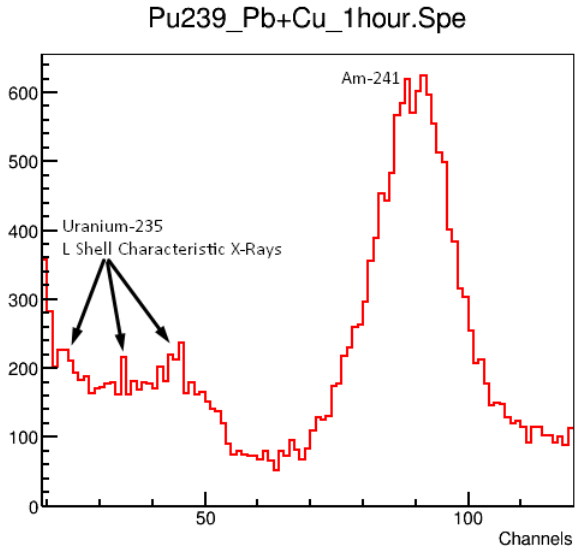

Figure 33. Zoomed Version of Figure 32

3.9. Dose Calculation of the Internal Exposure of ^{239}Pu

In case of intake of a radionuclide from a wound, it is generally washed away from the SHIELDING immediately. Therefore, in this study, it is assumed that the ^{239}Pu goes into only the blood circulation. It is also assumed that the route of intake is ingestion due to the lack of data for injection.

ICRP publication 119 report gives information about dose coefficients for intakes of radionuclides by workers and public.

Table 3. Effective Dose Coefficients (E) For Ingested ^{239}Pu for Workers

Nuclide	$T_{1/2}$	Ingestion		
		Type	f_1	e (Sv/Bq)
^{239}Pu	24065 (y)	M	0.0005	2.50E-07
		S	0.0001	5.30E-08

Data of Table 3 is taken from the table A.1 of ICRP publication 119 (ICRP, 2012). In table 3, M type means moderate rate of absorption of the material and S is the slow rate of absorption, f_1 is the fraction of an ingested element absorbed directly into body fluids and e is the effective dose coefficient. To find the effective dose delivered from the ^{239}Pu source directly to the blood;

$$E = A \times \frac{e}{f_1} \tag{3.1}$$

Where A is the activity of the source at the date of the experiment which is 23/07/2019. The activity of the source was 3700 Bq at 15/09/2014. So the A is determined as;

$$A = A_0 e^{-\lambda t} \tag{3.2}$$

Where A_0 is the initial activity, λ is decay constant and equal to $ln2/T_{1/2}$ and t is the time between the initial and experiment dates.

So the equation 3.1 becomes,

$$E = 3700\ Bq \times e^{-\frac{ln2}{24065 \times 365\ day} 5424\ day} \times \frac{2.7 \times 10^{-7} Sv/Bq}{0.0005}$$

$$E = 1.99\ Sv$$

This result exceeds the dose limit for workers, which is 20 mSv/year.

4. RESULTS AND DISCUSSION

4.1. The Comparisons of Background for All Shielding Geometries

When it is considered that a number of background data were taken, the comparison of all cases helps one to see the effect of different materials and geometries on background radiation. The comparisons are given in the following subsections;

4.1.1. Effect of Lead Shielding on Background

Figure 34 provides the comparison of energy spectra of three geometries are; background without a shielding, semi shielded geometry given in Figure 23 and absolutely shielded geometry given in figure 25. It is easily seen that the lead is very effective at reducing the background comes from the terrestrial radiation and the cosmic rays. However, the characteristic X-ray appears even without any source near the shielding.

In addition, the counting time was different for all three cases, to be able to see all cases in one plot, the counts were normalized to 500 seconds. Figure 34 shows the effect of lead on background radiation.

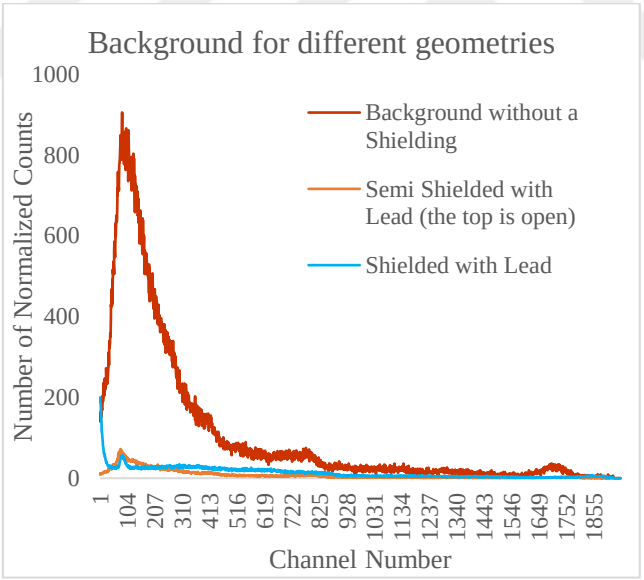

Figure 34. Background Radiation for Different Geometries

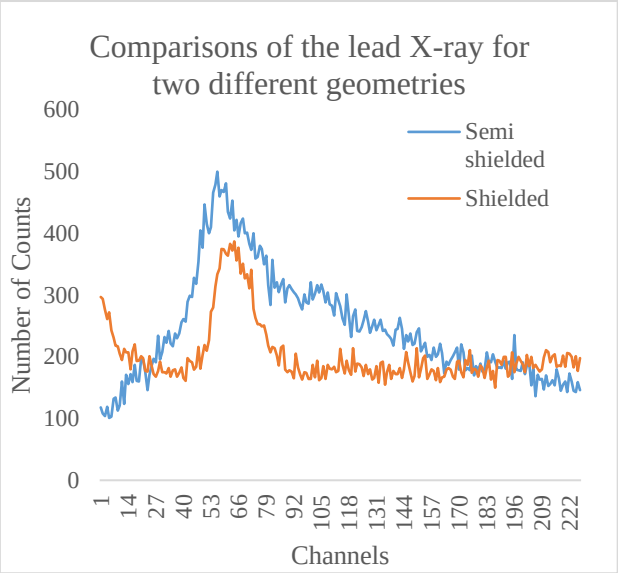

Figure 35. Closer Illustration of Figure 34

Figure 35 provides the comparison of the characteristic X-rays from semi shielded and totally shielded geometries. The totally closed geometry makes the background less while increases the contribution of the characteristic X-rays. This explains the necessity of the graded shielding on a low energy radiation measurement.

4.1.2. Effect of Different Graded Shieldings on the Characteristic X-Rays of Lead

The difference between two graded shieldings by providing the effect of them on the X-rays of lead is given in this section. Figure 36 gives the number of counts taken for one hour with lead and with iron shielding inside the lead, in the same way, figure 37 provides information of the change in characteristic X-ray of lead when copper is added. When figures 36 and 37 are compared, it is seen that the copper is more effective than iron on eliminating the X-rays from the lead because of its slightly higher density and atomic number as given in Table.2

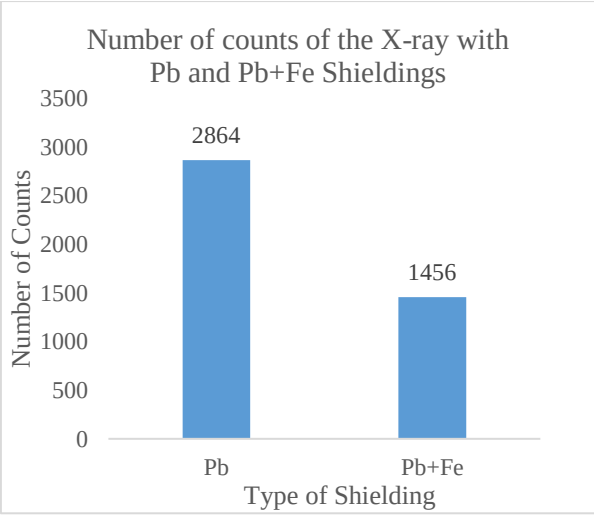

Figure 36. Comparison of the Number of Counts of Characteristic X-Rays of Lead for Pb and Pb+Fe Shieldings

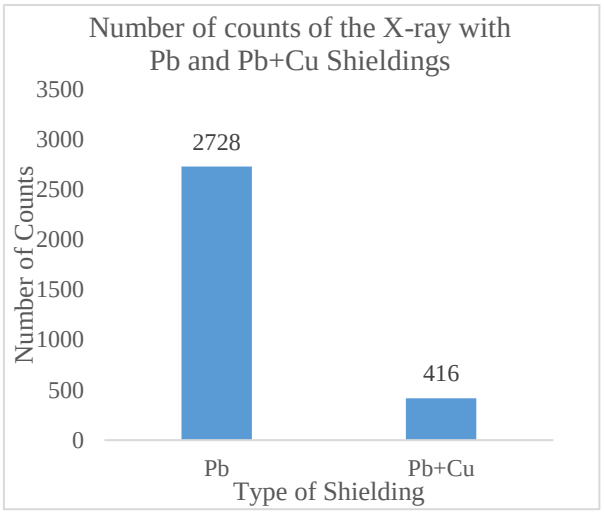

Figure 37. Comparison of the Number of Counts of Characteristic X-Rays of Lead for Pb and Pb+Cu Shieldings

Overall, copper will be preferred when taking the gamma-ray energy spectrum of a weak ^{239}Pu source.

4.2. ^{239}Pu Gamma Spectrum with Graded Shielding

Figure 38 illustrates the necessity of graded shielding when detecting low activity ^{239}Pu. It is seen that in the absence of copper inside the lead, it is impossible to see the Uranium L shell X-rays. In addition, with the help of copper, Americium peak can be detected accurately without any contribution from the characteristic X-rays of the lead.

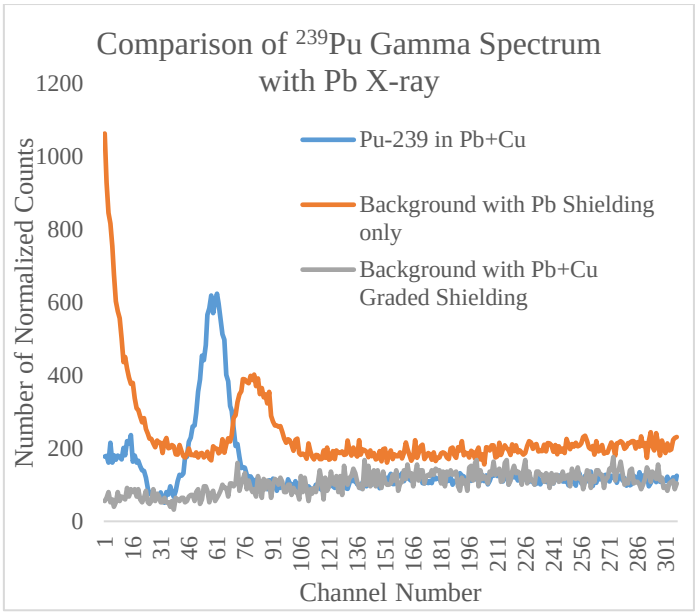

Figure 38. The Comparison of ^{239}Pu Gamma Spectrum with the Characteristic X-Rays of Lead

5. CONCLUSION

This study was undertaken to investigate the requirement of graded shielding to get a low background environment to enable low energy radiation to be measured. Since low background is needed while monitoring radionuclides, which usually ^{239}Pu is concern, taken into the body via a wound or cut on the skin, lead was used to shield the surrounding of the NaI(Tl) detector to create a detection system similar to a wound monitor and the characteristic X-rays of lead was trying to eliminate with a second lower Z material. Within this context, two different graded shieldings were built as; with lead plus iron and lead plus copper to observe the effect of the second material on the characteristic X-ray of lead and background radiation. The investigation of lining iron or copper inside the main lead shielding has shown that copper is more effective than iron on eliminating characteristic X-rays of lead.

A gamma spectrum of a low activity ^{239}Pu was taken inside the graded shielding with copper after calculating the MDA of the Americium peak appears on the ^{239}Pu spectrum. The MDA was founded as 672 ± 20.51 Bq, which is relatively low when compared with 3700 Bq ^{239}Pu. If this source had been accidentally taken from a wound on the body, the effective dose it would give was calculated as 1.99 Sv on 23/07/2019, which exceeds the annual dose limit for workers due to the high alpha emission of ^{239}Pu.

Overall, this study allows one to see the importance of reducing background radiation while measuring low-level radiation. Besides reducing the background, the results of this study support the idea that elimination of lead X-ray with a lower Z material is necessary for low-level radiation measurements and the evidence from this study suggests that lining copper inside the lead is more effective than iron. This result contributes to existing knowledge of graded shielding by providing a comparison of close Z number elements which are iron and copper. The evidence from this study suggests that NaI(Tl) detector with a graded shielding with copper can be used in a wound monitoring system.

The major limitation of this study is that the experiment was performed in an empty laboratory where is no contribution from other sources on the spectra except background**.** In a reprocessing plant or a busy laboratory, there will be different contributions to the background and the thicknesses of the shieldings used in this study may not be enough. Another limitation is limited efficiency at low energies due to the thick aluminum can surrounds the NaI crystal. If it were thinner, more accurate results could be found at low energies.

Further research can be carried out with HPGe while monitoring radionuclides since it has a better resolution than NaI(Tl). Also, considering that more than two-thirds of the human body consists of water, ^{239}Pu spectrum can be taken inside the water to calculate the effective dose delivered to the human body with injection.

REFERENCES

Browne, C.I. (1952) Precision Measurement of X-Rays and Gamma Rays in Radioactive Decay. Thesis.University of California:
Available at: http://inspirehep.net/record/896335/files/P00037419.pdf (Accessed: 15 August 2019).

Currie, L. A. (1968) Limits for Qualitative Detection and Quantitative Determination. *Anal. Chem.* Analytical Chemistry Division, National Bureau of Standards, Washington, D.C. 40(3), pp. 586-593.

Dimmerling, P.J. (2007) Characterization of Wound Monitoring Systems Used to Quantify and Locate Plutonium Contamination. Thesis. Texas A&M University.

Evans, R.D. (1955) *The Atomic Nucleus*. New York: McGrraw-Hill, Inc.

Firestone, R.B. (1996) *Table of Isotopes*. 8th edn. Edited by Virginia S. Shirley. Lawrence Berkeley National Laboratory, University of California: John Wiley & Sons, Inc. Volume 2.

Genicot, J.L., Hardeman, F., and Oberstedt, S. (1995) 'The Assessment of Plutonium and Americium in Contaminated Wounds with High Energy Resolution Semiconductor Detectors', *Pergamon*, 46(3), pp. 199-203.

Harduin, J.C., and Odilon, G. (1988) *The Detection of Contamination in Wounds*. Biological Laboratory, Cogema-La Hague Plant.

ICRP (1998) *Genetic Susceptibility to Cancer*. ICRP Publication 79. Annals of the ICRP, 28(1-2), pp. 1-157.

ICRP (2012) *Compendium of Dose Coefficients based on ICRP Publication 60*. ICRP Publication 119. Ann. ICRP 41(1), pp. 1-130.

Knoll, G.F. (2000) *Radiation Detection and Measurement.* 3th edn. United States of America: John Wiley & Sons, Inc.

Knoll, G.F. (2010) *Radiation Detection and Measurement*. 4th edn. United States of America: John Wiley & Sons, Inc.

Kuhn, H.G. (1969) *Atomic Spectra*. 2nd edn. London: Longman Group Limited.

National Aeronautics and Space Administration, Science Mission Directorate (2010) Gamma Rays. Available at: https://science.nasa.gov/ems/12_gammarays (Accessed: 20 July 2019).

Nelson, G., and Reilly, D. (1991) 'Gamma-Ray Interactions with Matter', Passive Nondestructive Analysis of Nuclear Materials, Los Alamos National Laboratory, pp. 27-42.

NNDC, Brookhaven National Laboratory (2019) *Interactive Chart of Nuclides.* Available at: https://www.nndc.bnl.gov/nudat2/ (Accessed: 15 August 2019).

Revink , A.R., and Khairi, M-S.A. (2018)' Background reduction by Cu/Pb shielding and efficiency study of NaI(TI) detector', Nuclear Engineering and Technology, 50, pp. 462-469.

Singh, V.P., Veerendra, D.D., Dileep, B.N., Sheikh, Q., Managanvi, S.S., Badiger, N.M., and Bhat, H.R. (2011) 'Background minimisation of HPGe detector by passive graded shielding', *International Journal of Low Radiation*, 8(4), pp. 313-328.

Suzuki-Yasumoto M., and Inaba, J. (1976) 'Absorption and metabolism of radioactive cobalt compound through normal and wounded skins', *National Institute of Radiological Sciences*, 6(18), pp. 119-136.

Tait, W. H. (1980) *Radiation Detection.* London : Butterworths.

Theodorsson, P. (1996) *Measurement Of Weak Radioactivity.* Singapore: Word Scientific Publishing Co. Pte. Ltd.

Till, J.E. and Grogan, H.A. (2008) *Radiological Risk Assessment and Environmental Analysis.* Oxford: Oxford University Press, Inc.

(2019) Available at: https://www.techopedia.com/definition/572/analog-to-digital-converter-adc (Accessed: 1 August 2019).

APPENDIX

Table 4. MSc Box 1 Source Activities

Isotope	ID	Activity (Bq)	Date Measured
^{60}Co	1U630	6240 ± 120	21/11/2013
^{133}Ba	1R545	45600 ± 2190	21/11/2013
^{137}Cs	1S684	191000 ± 7080	21/11/2013
^{152}Eu	1D157	83200 ± 4160	21/11/2013
^{241}Am	1Q598	415000 ± 20700	21/11/2013

Table 5. Data for Calibration and Resolution

sources	x (Energy)	y (Centroid)	Error Centroid	FWHM	Error FWHM	Resolution	ln(energy)	Ln(res)	error resolution	ln res error
^{60}Co	1173.228	1410.52	0.151584	76.2356	3.00E-01	0.054048	7.0675142	-2.917885	2.13E-04	3.94E-03
	1332.492	1598.99	0.166981	81.8387	0.323554	0.051181	7.1948062	-2.972377	2.02E-04	3.95E-03
^{137}Cs	661.657	811.965	0.00933739	61.6594	0.0184217	0.075938	6.4947473	-2.577832	2.27E-05	2.99E-04
^{241}Am	17.6	39.4536	0.00666811	19.8787	0.0212463	0.50385	2.8678989	-0.685476	5.45E-04	1.08E-03
	59.5409	83.3521	0.00177289	18.4149	0.00389553	0.220929	4.0866635	-1.509914	4.70E-05	2.13E-04
^{133}Ba	30.973	44.8405	0.00492195	12.6546	0.0112522	0.282214	3.4331159	-1.265091	2.53E-04	8.96E-04
	80.9979	111.937	0.012527	19.9635	0.0310036	0.178346	4.3944232	-1.724031	2.78E-04	1.56E-03
	295.42	379.704	0.0999634	25.4115	2.09E-01	0.066924	5.6883981	-2.70419	5.51E-04	8.23E-03
	356.0129	451.12	0.0336513	3.88E+01	0.0937054	0.085906	5.874967	-2.454505	2.08E-04	2.42E-03
	383.8485	565.96	0.121745	21.2795	0.207109	0.037599	5.9502479	-3.280779	3.66E-04	9.74E-03
^{152}Eu	40.1	58.6427	0.00515792	15.2965	0.0113994	0.260842	3.6913763	-1.343839	1.96E-04	7.50E-04
	121.7817	165.389	0.0097309	22.2201	0.022056	0.134351	4.8022301	-2.007303	1.34E-04	9.94E-04
	244.6974	315.999	0.0632175	22.6751	0.11609	0.071757	5.5000223	-2.634472	3.68E-04	5.12E-03
	344.2785	436.165	0.0201842	45.1545	0.49692	0.103526	5.8414509	-2.267931	1.14E-03	1.10E-02
	778.9045	955.001	0.110622	49.8522	0.210288	0.052201	6.6578884	-2.95265	2.20E-04	4.22E-03
	964.057	1180.014	0.16374	76.9109	0.38195	0.065178	6.8711504	-2.730634	3.24E-04	4.97E-03
	1100.52	1349	0.0919304	111.704	0.2192	0.082805	7.0035381	-2.491266	1.63E-04	1.96E-03
	1408.013	1717.62	0.136573	112.825	0.351038	0.065687	7.2499348	-2.722857	2.04E-04	3.11E-03

Table 6. Data of NaI(Tl) Efficiency Calculation

Sources	Gamma energies	Intensity %	Initial Activity	error on activity	counts (500 sec)	error on counts ±	S0	t1/2(day)	S	Intrinsic Efficiency	absolute Efficiency
60Co	1173	1.00	6240	120	81592	342.28	6230.64	1924.83	2969.44	54.95	27.48
	1332	1.00	6240	120	72132	314.01	6238.91	1924.83	2973.39	48.52	24.26
137Cs	662	0.85	191000	7080	9674170	3309.23	162541.00	11019.36	142804.50	135.49	67.74
241Am	18	0.20	415000	20700	5206290	7194.05	145623.50	171663.83	144418.41	72.10	36.05
	60	0.35	415000	20700	24200200	4948.51	145623.50	171663.83	144418.41	335.14	167.57
133Ba	81	0.33	45600	2190	1804410	1510.67	15002.40	3838.70	10346.00	348.81	174.41
	295	0.13	45600	2190	1093700	1281.99	5814.00	3838.70	4009.47	545.56	272.78
	356	0.62	45600	2190	121418	1171.83	28294.80	3838.70	19512.75	12.44	6.22
	384	0.09	45600	2190	1160190	3518.61	4076.64	3838.70	2811.35	825.36	412.68
152Eu	40	0.38	83200	4160	2430220	1885.32	31948.80	4936.61	23930.94	203.10	101.55
	122	0.29	83200	4160	1664500	1555.60	23736.96	4936.61	17779.94	187.23	93.62
	245	0.08	83200	4160	146632	827.18	6281.60	4936.61	4705.17	62.33	31.16
	344	0.27	83200	4160	1643880	1635.89	22122.88	4936.61	16570.93	198.41	99.20
	779	0.13	83200	4160	201113	900.20	10757.76	4936.61	8057.99	49.92	24.96
	964	0.15	83200	4160	282274	1108.70	12072.32	4936.61	9042.65	62.43	31.22
	1101	0.12	83200	4160	221189	1043.75	9892.48	4936.61	7409.87	59.70	29.85
	1408	0.21	83200	4160	340077	1203.40	17363.84	4936.61	13006.21	52.29	26.15

Table 7. Probability of Occurrence of Given Deviations Predicted by the Gaussian Distribution

ε_0	t_0	$f(t_0)$
0	0	0
0.674 σ	0.674	0.500
σ	1.00	0.683
1.64 σ	1.64	0.900
1.96 σ	1.96	0.950
2.58 σ	2.58	0.990
3.00 σ	3.00	0.997